Applied Catalysis B: Environmental 147 (2014) 330–339

Contents lists available at ScienceDirect

Applied Catalysis B: Environmental

journal homepage: www.elsevier.com/locate/apcatb

Cu/Cu_xO and Pt nanoparticles supported on multi-walled carbon nanotubes as electrocatalysts for the reduction of nitrobenzene

Xia Sheng[a,1], Benny Wouters[b,1], Tom Breugelmans[b], Annick Hubin[b], Ivo F.J. Vankelecom[a], Paolo P. Pescarmona[a,*]

[a] Centre for Surface Chemistry and Catalysis, University of Leuven (KU Leuven), Kasteelpark Arenberg 23, PO Box 2461, 3001 Heverlee, Belgium
[b] Vrije Universiteit Brussel, Research Group Electrochemical and Surface Engineering, Pleinlaan 2, 1050 Brussels, Belgium

ARTICLE INFO

Article history:
Received 7 July 2013
Received in revised form 29 August 2013
Accepted 6 September 2013
Available online 14 September 2013

Keywords:
Copper
Nanoparticles
Multi-walled carbon nanotubes
Electrocatalyst
Nitrobenzene

ABSTRACT

Cu/Cu_xO and Pt nanoparticles supported on multi-walled carbon nanotubes (MWCNTs) were studied as electrocatalysts for the reduction of nitrobenzene in a half-cell set-up. This reaction not only produces valuable chemicals, but has the potential to generate electricity if applied in a fuel cell device. MWCNTs with and without functional groups were investigated as supports for the nanoparticles, employing either ethylene glycol (EG) or H_2 gas as reductant. Cu/Cu_xO nanoparticles supported on pristine multi-walled carbon nanotubes prepared using H_2 as reductant ($Cu/MWCNT\text{-}H_2$) were identified as the best electrocatalyst for the reduction of nitrobenzene on the basis of its onset potential and of the number of electrons transferred per nitrobenzene molecule. This material consists of well-dispersed Cu/Cu_xO nanoparticles with an average size of 8 nm. The stability of $Cu/MWCNT\text{-}H_2$ was tested by cyclic voltammetry (CV) for 1000 cycles, showing that the activity of this electrocatalyst does not deteriorate over time. The electrochemical reduction of nitrobenzene over $Cu/MWCNT\text{-}H_2$ in acidic ethanolic medium at −0.62 V vs. Fc/Fc^+ led to 44% conversion with an overall selectivity toward azoxybenzene (AOB) of 82%.

© 2013 Elsevier B.V. All rights reserved.

1. Introduction

Great efforts are currently being devoted to the development of alternative ways to produce energy. Fuel cells are an attractive option as they can convert chemical energy directly into electricity without combustion processes, so that high efficiencies in terms of energy conversion might be achieved. The most widely studied fuel cells are the H_2/O_2 fuel cell and the direct methanol fuel cell, with water and CO_2 as end products, respectively [1]. A different, highly attractive but much less investigated type of fuel cells is that in which industrial chemicals of high interest are produced while electricity is generated [2]. In the chemical industry, many relevant products are prepared through thermodynamically favorable reactions ($\Delta G < 0$) and the produced energy (if $\Delta H < 0$) is generally dissipated in the form of heat. In integrated production sites, this heat can be exploited in neighboring processes or via heat-exchangers, but often this heat is just wasted. In the worst case, it might even induce important cooling costs or lower reaction yields due to presence of reactor hot spots [3]. If the same reactions were performed in a fuel cell configuration, this energy could be employed favorably to generate electricity together with the desired chemical products, thus greatly improving the sustainability and the economics of the process. In this work, an electrocatalyst for such electrochemical cogeneration approach is developed for the reduction of nitrobenzene and evaluated in a half-cell set-up. All products of this reaction have a broad range of applications: particularly, aniline is largely employed as reagent for the synthesis of polyurethanes [4], and azoxybenzene (AOB) is an important azo compound in organic syntheses [5].

Since the early work of Haber published at the turn of the 19th century, the electrochemical reduction of the aromatic nitro group has been studied extensively [6,7]. In acidic and neutral solution the reaction proceeds by consecutive electrocatalytic hydrogenation steps, as summarized in Scheme 1 [8]. The first 2-electron exchange step leads to the formation of the intermediate nitrosobenzene (NSB), which cannot be isolated under most conditions, because of its fast conversion to phenylhydroxylamine (PHA) through further 2-electron reduction [9]. A third 2-electron reduction step involves the conversion of PHA to aniline and is favored in weakly acidic solution [8]. PHA is a very unstable compound, and besides being an intermediate in the aniline-NSB redox-related pair, it can undergo three competitive chemical reactions (Scheme 1): (1) disproportionation into aniline and NSB (blue) [10], (2) conversion to *p*-ethoxyaniline through the Bamberger rearrangement in strong acidic environment (green) [11], (3) oxidation to NSB followed by condensation of NSB with another PHA molecule to produce AOB (red) [12]. The electrochemical reduction of nitrobenzene to

* Corresponding author. Tel.: +32 16 321592.
E-mail address: Paolo.Pescarmona@biw.kuleuven.be (P.P. Pescarmona).
[1] These authors contributed equally.

0926-3373/$ – see front matter © 2013 Elsevier B.V. All rights reserved.
http://dx.doi.org/10.1016/j.apcatb.2013.09.006

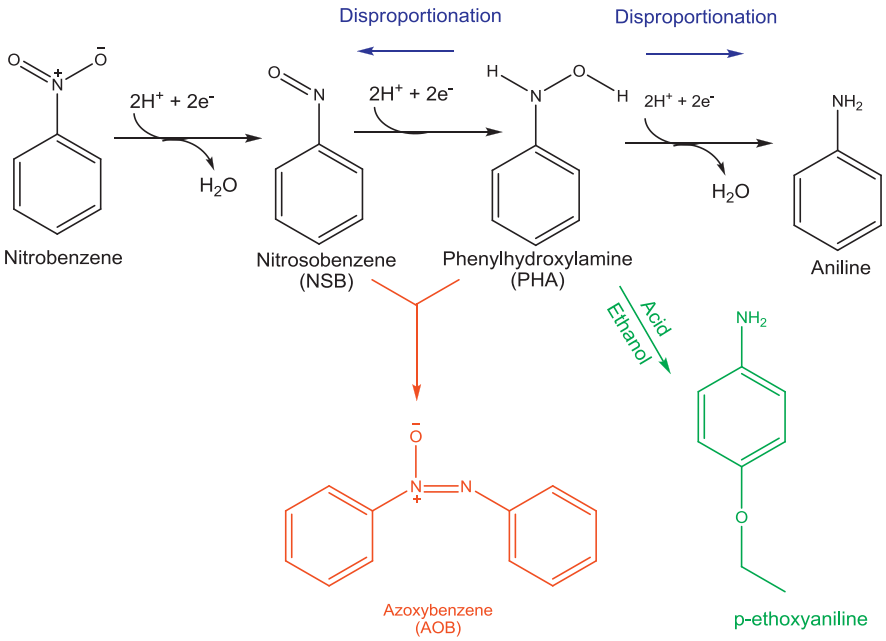

Scheme 1. Reduction of nitrobenzene.

aniline, and its further electrochemical hydrogenation to cyclohexylamine, have been studied by Yuan et al. in a fuel cell reactor for cogeneration of chemicals and energy [2]. The products of the reduction of nitrobenzene are strongly related to the nature of the electrode [8,11,13] and to the reaction conditions, such as pH [8,13], solvent [14,15] and applied electrical potentials [11,14]. Therefore, the control of the reaction conditions is of crucial importance for obtaining the desired product. In this work, the electrochemical reduction of nitrobenzene in neutral or acidic ethanolic medium is reported, by using $LiClO_4$ or $HClO_4$ as supporting electrolytes in a half-cell set-up. With the aim of evaluating the activity of the electrocatalysts for the cathode reaction in conditions that could also be employed at a later stage in a fuel cell set-up, only an acidic or neutral medium can be considered, since the oxidation of hydrogen supplying protons would be the anodic reaction in the fuel cell.

Since electrochemical reactions occur through the interaction between the electrocatalyst surface and the reagent, the physicochemical features of the electrocatalyst are of critical importance. Noble metals have been often reported as highly stable and active electrocatalysts, especially Pt and Pd [2,16]. However, their cost is a serious drawback. Cu has been investigated as a less expensive alternative to noble metals. In the electrochemical reduction of nitrobenzene, Cu-based electrocatalysts have been reported to display promising catalytic activity [2,13]. Different forms of Cu-based metal electrodes have been employed in these studies: bulk Cu metal [17], Cu-based alloys [8], polycrystalline Cu [18] and Devarda Cu [13]. In this work, Cu and Pt nanoparticles supported on MWCNTs are studied for the first time as electrocatalysts for the electrochemical reduction of nitrobenzene. This study focuses on the design and development of these electrocatalysts and is complemented by a recent report from our groups in which the most suitable electrochemical methods and conditions for performing the reduction of nitrobenzene were identified, and the reaction mechanism was investigated [19]. The use of nanoparticles supported on an electron-conductive material is receiving great attention for electrocatalytic applications [20], particularly in the case of the expensive noble metals, because the small size of the particles implies a larger active area per gram of metal compared to bulk metal electrodes. This can lead to very good performances with a much lower amount of metal, provided that the nanoparticles have small and uniform size and that they are homogeneously dispersed on the surface of the support [20]. MWCNTs were selected as support material, because they are good electrical conductors (electrical conductivity = 10^5–10^7 S m^{-1}) due to the extended delocalization of electrons in the π-orbitals, have a high tensile strength, and display an excellent resistance to electrochemical corrosion [21]. Different synthetic approaches were employed to prepare the supported Cu nanoparticles, in order to optimize the nanoparticle size and dispersion toward the best electrocatalytic performance. In the preparation of these materials, the challenge does not only consist in controlling the particle size and distribution, but also in defining the most suitable Cu species for the electrocatalytic application. The synthesis and use of exclusively metallic Cu nanoparticles supported on high surface area conductive carbon materials has been limited by the electrochemical instability of metallic Cu against oxidation [22]. However, it has been proposed that Cu_2O and CuO species can act as active sites in electrochemical reactions [23]. Therefore, both the nature of the Cu species and the morphology and size of the particles were investigated and correlated to the electrocatalytic properties of the materials in this study. The activity of the different Cu and Pt electrocatalysts in the nitrobenzene reduction was compared by means of electrochemical measurements.

2. Experimental

2.1. Preparation of Pt and Cu electrocatalysts

All chemical reagents were of analytical grade and used as received without purification. The commercial MWCNTs (Nanocyl NC 7000, purity > 90%; provided by 'Nanocyl', Belgium) have an average internal diameter of 9.5 nm, a length of 20–50 nm and a BET surface area of 323 m^2 g^{-1}. These nanotubes were functionalized (MWCNT-F) by means of an oxidation treatment performed by suspending and stirring them in a 1:3 solution of sulfuric acid (98 wt%) and nitric acid (aq., 70 wt%) for 24 h. Next, the MWCNT-F were washed with distilled water to neutral pH and dried in an oven overnight at 100 °C. The treatment with a 1:3 mixture of H_2SO_4 and HNO_3 was employed in this work as this has been reported to generate the most abundant density of surface –COOH and the highest

oxidation resistance [24]. The BET surface area of the MWCNT-F sample was measured by N_2 physisorption as 313 $m^2 g^{-1}$. The N_2 adsorption/desorption isotherms at 77 K were measured on a Micrometrics Tristar 3000.

Supported Pt nanoparticles were prepared by modification of a previously reported method [25,26], in which ethylene glycol (EG) was employed as reductant and sodium acetate as stabilizer of the metal particles. The theoretical metal loading of Pt was 20 wt%. The desired amounts of aqueous solutions of $H_2PtCl_6{\cdot}6H_2O$ (0.1 M) and sodium acetate (1.0 M, seven times the number of moles of Pt) were added to a stirred suspension of 80 mg of MWCNT-F or MWCNT in 40 ml of EG/water solution (1:1 in vol.). The mixture was homogenized by ultrasound for at least 1 h, and then refluxed at 170 °C in an oil bath for 4 h under Ar flow. The resulting suspension was filtered. The residue was washed with distilled water to remove the acetate ions, and acetone to wash off the organic solvent. The solid product was dried overnight at 100 °C in a vacuum oven (Pt/MWCNT-F-EG and Pt/MWCNT-EG).

Supported Cu/Cu_xO nanoparticles with a theoretical Cu-loading of 20 wt% were prepared according to two different methods. Both untreated and functionalized MWCNTs were employed as support. The first method is similar to that used for the preparation of the supported Pt nanoparticles described above, with EG as reductant. $CuSO_4{\cdot}5H_2O$ (0.05 M) was used as a precursor. The obtained electrocatalysts were named Cu/MWCNT-F-EG and Cu/MWCNT-EG. The second method is based on wet impregnation, with $Cu(NO_3)_2$ as precursor instead of the commonly used $CuCl_2$, because chloride can have a negative effect in electrochemical processes [27]. An aqueous solution of $Cu(NO_3)_2{\cdot}3H_2O$ (0.05 M, 6.3 ml) was added to a suspension of carbon (80 mg) in 30 ml H_2O, and stirred for 24 h. Next, the solvent was removed by using a rotary evaporator. The solid residue was treated in a quartz U-tube at 200 °C under N_2 for 2 h and reduced by H_2 (flow rate of 1 $cm^3 s^{-1}$) at 140 °C for 1 h. The electrocatalysts obtained by this method are denoted as $Cu/MWCNT\text{-}F\text{-}H_2$ and $Cu/MWCNT\text{-}H_2$.

2.2. Physical and chemical characterization of Pt and Cu electrocatalysts

The morphology and size of the nanoparticles dispersed on the surface of the carbon supports were investigated by transmission electron microscopy (TEM) and powder X-ray diffraction (XRD). TEM was performed on a Philips FEG CM200 operating at 200 kV. The average size of particles was manually determined by TEM measurements by counting 100 particles, and the standard deviation was calculated covering 90% particles. XRD patterns were measured on a STOE Stadi P instrument using Cu $K\alpha$ radiation ($\lambda_{K\alpha}$ = 0.154 nm). For the XRD measurement, the powder samples were placed in a glass capillary (0.5 mm of diameter). The diffraction peaks were used to estimate the mean size of metal particles according to Scherrer's formula [28]: $L = 0.9\lambda_{K\alpha}/(\beta_{2\theta}\cos\theta)$. Where L is the mean size of the nanoparticles, θ is the angle of the peak and $B_{2\theta}$ describes the half-peak width for the peak (in radians). The grain sizes of Pt was determined from the measurement of the (2 2 0) peaks; for the Cu/Cu_xO nanoparticles the dominating peak in each sample was used. The ICDD database was employed to identify the crystalline phases [29]. X-ray photoelectron spectroscopy (XPS) measurements of Cu/Cu_xO nanoparticles were carried out with a Physical Electronics PHI 1600 multi-technique system using Al $K\alpha$ (1486.6 eV) monochromatic X-ray source, which was operated at 15 kV and 150 W at a basis pressure of 2×10^{-9} Torr. In order to correct possible deviations caused by electric charge of the samples, the graphitic C 1s band at 284.6 eV was taken as internal standard. The regional XPS signals of Cu 2p were deconvoluted by using the multipack software to recognize different oxidation states of the metals on carbon. The metal contents were measured by energy dispersion X-ray spectroscopy (EDX) on a NORAN System SIX X-ray spectrometer (Thermo Scientific). The carbon-supported electrocatalysts were placed on an indium foil to avoid interference by the carbon from the sample holder. More than three zones in each sample were selected and the average values were reported. Temperature programmed desorption (TPD) was employed to analyze the oxygen-containing functional groups on MWCNT-F. The measurement was performed on a Quadrupole Mass Spectrometer Gas Analyzer with a Channeltron/Faraday detector. A sample of 25 mg was loaded in a quartz sample holder under a helium flow (20 $cm^3 min^{-1}$), heating from room temperature to 1000 °C at a rate of 10 °C min^{-1}.

2.3. Electrochemical tests

All the electrochemical measurements were carried out in a half-cell set-up using an Autolab 302N potentiostat or a BioLogic VMP3 multichannel potentiostat. Porous rotating disc electrodes were used for all electrochemical measurements. Catalyst ink solutions were prepared by dispersing 8.0 mg of electrocatalyst in 300 μl of 1% polystyrene solution in toluene. A 5 μl drop of this ink was deposited on a glassy carbon electrode, and dried at 50 °C for 20 min. Three replicate electrodes were prepared for each electrocatalyst, and the average catalyst loading was 0.45 mg cm^{-2}. The presence of oxygen in the electrolyte was minimized by bubbling nitrogen gas through the solution for 15 min. The counter electrode was a Pt grid, and the reference electrode was an Autolab saturated LiCl Ag/AgCl electrode. The exact potential of the reference electrode was measured by cyclic voltammetry of the ferrocene/ferrocenium (E°_{Fc/Fc^+} = −0.64 V vs. S.H.E) reference couple. All potentials in this paper are referred to this redox couple.

For linear sweep voltammetry (LSV) analysis, the concentration of nitrobenzene was 5 mM in 50 ml of solution, and a scan rate of 5 mV s^{-1} was used. The potential was varied from −0.3 V to −2.4 V vs. Fc/Fc^+.

Every measurement was repeated at least three times, in order to improve the reliability of the results. These electrochemical measurements for nitrobenzene reduction were carried out in neutral ethanolic electrolyte. The neutral solution contained 0.2 M $LiClO_4$ as support electrolyte in absolute ethanol. The resistance of the electrolyte between the reference electrode and the working electrode was determined to be 190 Ω [19]. The number of electrons transferred (n) was calculated by means of the Koutécky–Levich equation at −1.3 V vs. Fc/Fc^+ [19]. This equation was also used to estimate the kinetic current for the two electrocatalysts for which four electrons were exchanged ($Cu/MWCNT\text{-}H_2$ and Cu/MWCNT-EG). The onset potential for each electrocatalyst was calculated as the potential at which the slope of the voltammogram exceeded 0.1 mA V^{-1}. At least three electrodes were prepared and measured for each electrocatalyst and the 95% confidence interval was calculated for the onset, assuming the values to be distributed as a Student-t distribution.

The electrochemical stability for selected electrocatalysts was tested using cyclic voltammetry (CV). In a 0.2 M $LiClO_4$ solution, the potential was cycled between −0.3 V and −1.7 V vs. Fc/Fc^+. The scan rate was set at 100 mV s^{-1}. A number of 1000 cycles were carried out and the difference between the first and the last scan was examined. The solution was stirred again before the last scan in order to homogenize the concentration of nitrobenzene in solution, thus increasing the comparability of the starting and final reaction conditions.

The nitrobenzene conversion and the products distribution produced by the most promising electrocatalyst were studied by means of chronoamperometric tests [19]. The reduction of nitrobenzene (15 mM) was carried out both in neutral (0.2 M $LiClO_4$) and acidic (0.3 M $HClO_4$) medium. In neutral medium, the

reaction was carried out at −1.15 V vs. Fc/Fc^+ for 46 h; in acidic medium, the reaction was performed at −0.62 V vs. Fc/Fc^+ for 52 h. The rotation speed of the working electrode was set at 500 rpm. The solution obtained from each chronoamperometric experiment was adjusted by 1 M KOH aqueous solution until the pH was between 4 and 5, neutralized by phosphate buffer solution (pH = 7, Fisher), and filtered to remove the insoluble $KClO_4$. The concentration of nitrobenzene and of the reaction products were measured by HPLC according to a procedure reported in detail elsewhere [29]. Each analysis was done in triplicate, and the average of the quantification results was reported.

3. Results and discussion

3.1. Synthesis and characterization of Cu/Cu_xO and Pt nanoparticles supported on MWCNTs

Cu/Cu_xO and Pt nanoparticles were supported on multi-walled carbon nanotubes. The MWCNTs were employed as such or after functionalization by acid treatment, which generates (–OH), (>C=O) and (–COOH) groups on the surface of the nanotubes (as determined by TPD, see Fig. S.2) [30]. These functional groups provide sites for anchoring the metal particles and can favor the dispersion of the nanotubes in polar organic solvents (see Fig. S.1). However, there are also some disadvantages of this treatment, since the oxidation can partially damage the structure of the carbon nanotube, causing a decrease in their electrical conductivity and corrosion resistance [24,31]. The acidic treatment also results in the opening of the tube tips and the cutting of the long tube into shorter species: deposition of metal particles may thus occur on the external walls but also in the interior of the nanotubes. If the metal particles are small enough, the reactants can diffuse through the channels and contact the metal particles. On the other hand, large particles may block the tubes causing the active surface areas to decrease. The functional groups on the surface of the MWCNT-F could react under an applied potential during the electrochemical process, leading to partial destruction of the material and/or blockage of the active sites of the electrocatalyst.

An ideal electrocatalyst based on supported metal nanoparticles would consist of small particles with a uniform size distribution and a good dispersion on the support surface (i.e. with no particle aggregates). Suitable Pt nanoparticles were successfully prepared using EG as reductant, according to a previously reported procedure in which sodium acetate is used to stabilize the Pt particles [26]. The acetate anions form a complex with the metal particles via their carboxylic groups, generating negatively charged particles that repel each other, thus favoring their dispersion and controlling their growth [26]. Hence, a material with isolated small particles can be formed. Another important factor influencing the dispersion of the nanoparticles is the viscosity of the solvent used in their synthesis [32]. A combination of EG and water with a 1 to 1 volume ratio was employed, as this mixture has been reported to provide the most suitable viscosity [25]. Indeed, using these conditions, a good dispersion of small Pt nanoparticles with uniform small size (2.9 ± 0.1 nm) was obtained on the external surface of the MWCNT-F, as shown by TEM (Pt/MWCNT-F-EG, Fig. 1a). The high density of functional groups on the external surface of the nanotubes, and more possible defect sites generated by the strong oxidative treatment have been proposed to facilitate the adsorption of the metal precursor and, thus, lead to a good dispersion of Pt particles on the surface [33]. On the other hand, Pt aggregates were observed in the TEM image of Pt/MWCNT-EG (Fig. 1b), and the size of the metal particles is less uniform (2.6 ± 1.1 nm), because there are no chemical active sites for anchoring isolated Pt nanoparticles on the surface of non-functionalized MWCNTs.

In the synthesis of supported Cu/Cu_xO nanoparticles, two different reductants were employed: a mild reductant as ethylene glycol (EG), like in the preparation of the Pt-based material (vide

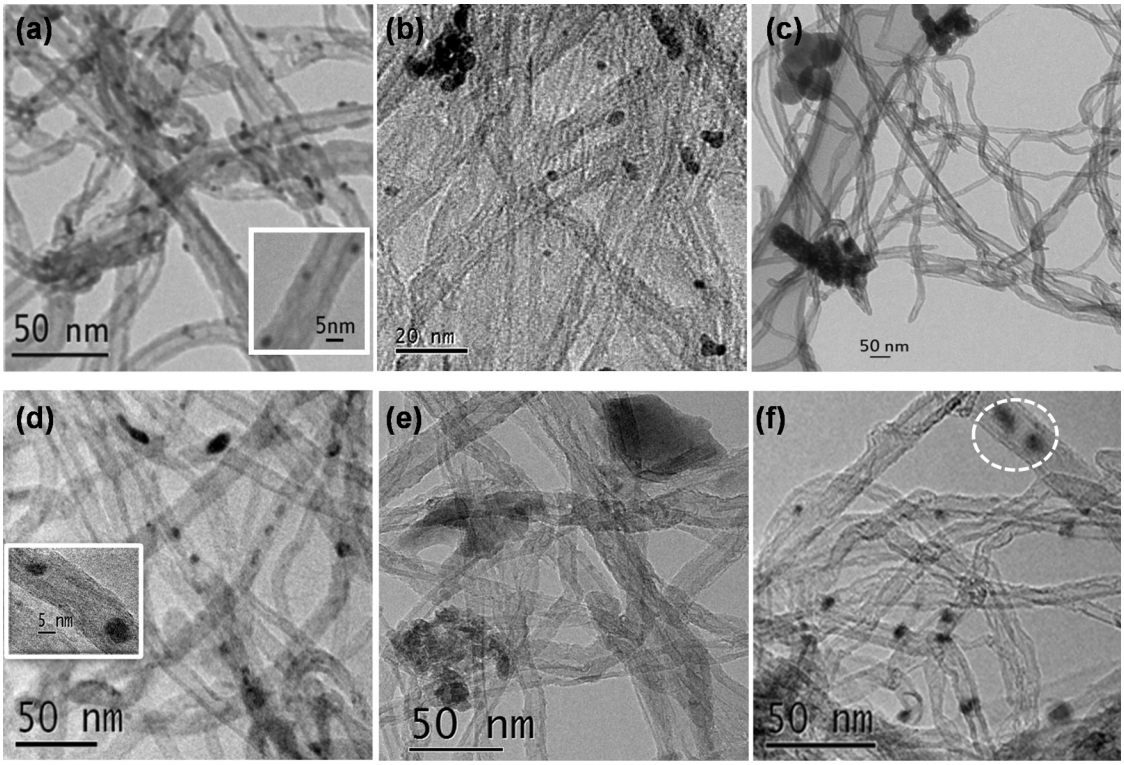

Fig. 1. TEM images of (a) Pt/MWCNT-F-EG; (b) Pt/MWCNT-EG; (c) Cu/MWCNT-F-EG; (d) Cu/MWCNT-F-H_2; (e) Cu/MWCNT-EG; (f) Cu/MWCNT-H_2. The insets evidence the location of the particles on the external surface (Pt/MWCNT-F-EG) or within the nanotubes (Cu/MWCNT-F-H_2).

Table 1
Metal loading, particle size and structure of the studied electrocatalysts.

Electrocatalyst[a]	EDX metal content [wt%]	XPS metal content [wt%]	Crystal phases (XRD)	Major Cu phase (XPS)	Particle Size [nm]	
					XRD[b]	TEM
Pt/MWCNT-F-EG	20	–	Pt(0)	–	3	2.9 ± 0.1
Pt/MWCNT-EG	20	–	Pt(0)	–	3	2.6 ± 1.1
Cu/MWCNT-F-EG	13	9	$Cu(OH)_2$, Cu_2O	$Cu(OH)_2$	n.d.	Aggregates
Cu/MWCNT-F-H_2	17	4	Cu(0), CuO, Cu_2O	CuO, $Cu(OH)_2$, Cu/Cu_2O	n.d.	*W*: 5 ± 4 *L*: 7 ± 5
Cu/MWCNT-EG	15	15	$Cu(OH)_2$, Cu_2O	$Cu(OH)_2$, Cu/Cu_2O	n.d.	Aggregates
Cu/MWCNT-H_2	15	15	Cu(0), CuO	CuO, $Cu(OH)_2$, Cu/Cu_2O	7	8 ± 3

MWCNT-F: functionalized MWCNTs; -EG: the reductant was EG; -H_2: the reductant was H_2; n.d.: not determined.
[a] The theoretical metal loading of all electrocatalysts is 20 wt%.
[b] The particle size determined from XRD analysis is only an indicative value, due to the relatively low resolution of the XRD measurements.

supra), and hydrogen gas, which has a higher reducing ability. Both the untreated and the functionalized MWCNTs were used as supports. TEM images show that large Cu particles were formed in Cu/MWCNT-F-EG and Cu/MWCNT-EG (Fig. 1c and e), indicating an aggregation of the metal. On the other hand, the synthesis of Cu electrocatalysts with H_2 as reductant gave much smaller Cu/Cu_xO nanoparticles (<10 nm) with a homogeneous dispersion on the support (Fig. 1d and f). These differences in particle size and distribution can be explained by considering that the preparation involving ethylene glycol was performed under stirring in an aqueous environment at an elevated temperature (170 °C). Under these conditions, Cu precursors could be transformed to Cu hydroxides (vide infra) and undergo aggregation. In contrast, in the method involving H_2 as reductant, the solvent is removed prior to the reduction step, which is carried out statically and at lower temperature (120 °C): these conditions favor the small size and high dispersion of the Cu/Cu_xO nanoparticles. Besides the effect of the reductants, the size and distribution of the particles is also influenced by the selected supports. Cu/MWCNT-H_2 exhibits a good dispersion of the nanoparticles, a rather small average particle size and a moderately broad size distribution (8 ± 3 nm, Fig. 1f). Remarkably, this synthetic procedure generates smaller Cu/Cu_xO nanoparticles compared to previously reported wet chemical approaches [34]. Most particles are deposited on the external surface but a small fraction is located inside the MWCNTs (see circled zone in Fig. 1f). The diffusion of the metal into the tubes is enhanced by changing the support from MWCNTs to the MWCNT-F. The acid treatment used to prepare MWCNT-F leads to a short and uncapped tube structure, which is more favorable for the diffusion and encapsulation of the Cu/Cu_xO nanoparticles in the nanotube. Indeed, most particles in sample Cu/MWCNT-F-H_2 are located within the nanotubes (Fig. 1d). Due to this spatial confinement, the growth of the nanoparticles is limited to a width that is smaller than the diameter of the carbon nanotube (average internal diameter of 9.5 nm). The particles could only grow along the tube, forming elongated shapes rather than being spherical (Fig. 1d), with a width of 5 ± 4 nm and a length of 7 ± 5 nm. The large majority of the particles in Cu/MWCNT-F-H_2 are encapsulated within the nanotubes, while in the other materials using MWCNT-F as support (Cu/MWCNT-F-EG and Pt/MWCNT-F-EG), the particles are preferentially located on the external surface. This is ascribed to the different procedure used to separate the sample from the solvent in the methods using H_2 and EG as reductant. The procedure with H_2 involves removal of the solvent by rotary evaporator, which could drive the Cu precursor into the tubes, followed by the particle formation and growth.

The physicochemical properties of all the studied samples are summarized in Table 1. The metal loading was estimated by EDX analysis: the Pt loading is consistent with the nominal amount in solution, while the content of Cu is generally lower than the theoretical value (20 wt%), indicating that some unreduced Cu precursor stayed in solution and was removed together with the solvent. XPS was also applied to detect the metal loading of the Cu electrocatalysts. Both EDX and XPS are surface analytical techniques: the maximum depth that can be analyzed by EDX is 2–3 μm, but only a 3 nm depth can be measured by XPS. It is interesting to notice that the results obtained with XPS correlate well with those by EDX when MWCNTs were used as the support. However, some discrepancies were observed for the Cu/Cu_xO particles supported on MWCNT-F, for which XPS gives much lower metal loading than EDX. This can be explained considering that part of the Cu/Cu_xO nanoparticles are encapsulated inside the MWCNT-F, as evidenced by TEM (vide supra). The wall thickness of the nanotubes is about 3.5 nm, implying that particles located within the tubes will not be detected by XPS. The discrepancy is more pronounced for Cu/MWCNT-F-H_2, i.e. the material with the largest fraction of encapsulated particles.

The structural features of the electrocatalysts were investigated by powder XRD (Fig. 2). The wide diffraction peak at $2\Theta = 25°$ for these electrocatalysts is characteristic of the highly graphitic structure (0 0 2) of the carbon nanotube support [31]. The presence of Pt particles in the Pt electrocatalysts is demonstrated by the diffraction peaks at $2\Theta = 39.8°$ (1 1 1), 46.4° (2 0 0) and 67.8° (2 2 0), which can be indexed to face-centered cubic (fcc) metallic Pt [26]. The broad diffraction peaks of the Pt particles in Pt/MWCNT-F-EG (Fig. 2a) are an indication of a small average grain size, estimated to be around 3 nm, in excellent agreement with the TEM analysis (Table 1). The XRD pattern of Pt/MWCNT-EG (Fig. 2b) exhibits broader diffraction peaks than Pt/MWCNT-F-EG, in line with the smaller particle size of Pt evidenced by TEM (Table 1). On the basis of these results, it can be concluded that the employed method with sodium acetate as stabilizer was successful for preparing supported Pt nanoparticles with the desired good dispersion of small nanoparticles with narrow size distribution.

XRD analysis of the Cu-based particles supported on untreated and functionalized MWCNTs reveals the presence of different crystalline phases (Fig. 2c–f). A typical XRD pattern of Cu(0) nanoparticles is characterized by peaks at $2\Theta = 43.3°$, 50.4° and 73.4°, which correspond to the (1 1 1), (2 0 0) and (2 2 0) planes of a face-centered cubic (fcc) structure (00-004-0836) [29,35]. When H_2 was used as the reductant and untreated MWCNTs as support (Cu/MWCNT-H_2), the XRD pattern (Fig. 2d) shows, besides metallic Cu, the peaks belonging to monoclinic CuO (01-080-1916) [22,29], which indicates that Cu(0) nanoparticles coexist with CuO in this sample. The presence of CuO is attributed to the incomplete reduction of the divalent metal ion in the precursor or to re-oxidation of metallic Cu. The average grain size of Cu/MWCNT-H_2 was calculated by Scherrer's equation to be around 7 nm, which is in the range of particle size determined by TEM (Table 1). The XRD pattern of Cu/MWCNT-F-H_2 (Fig. 2c) indicates that this sample is largely amorphous, though the main peaks corresponding to Cu, CuO and Cu_2O (01-071-3645) [29] can be recognized. This indicates the low degree of crystallinity of the particles inside the tubes, which are the

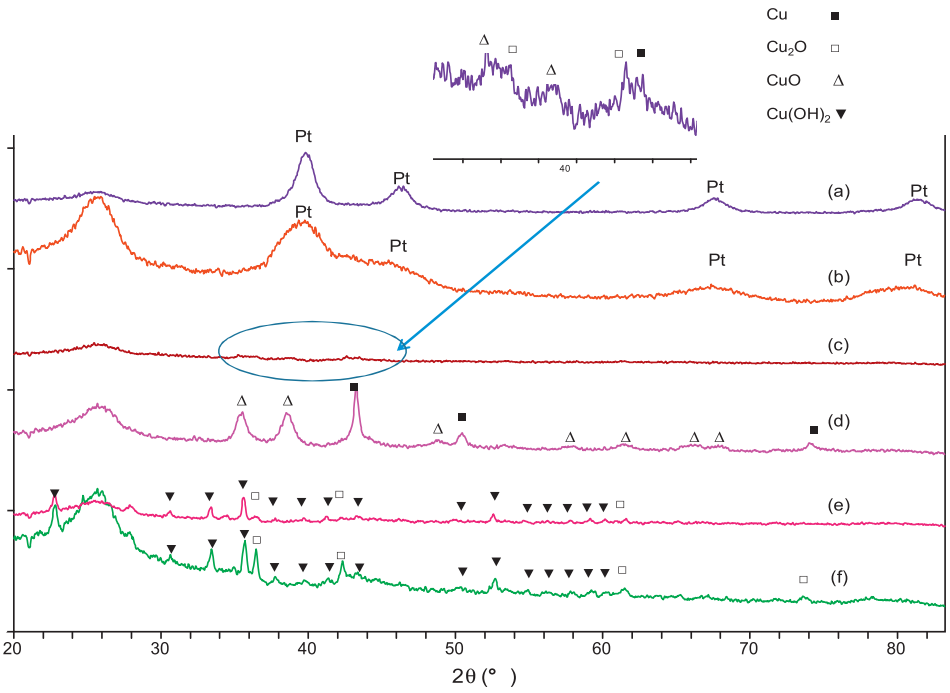

Fig. 2. XRD patterns of (a) Pt/MWCNT-F-EG; (b) Pt/MWCNT-EG; (c) Cu/MWCNT-F-H_2; (d) Cu/MWCNT-H_2; (e) Cu/MWCNT-F-EG; (f) Cu/MWCNT-EG.

prevalent species in this sample (vide supra). Such poor crystallinity might be ascribed to the confined growth of the particles inside the nanotube. The Cu/Cu_xO electrocatalysts prepared with EG as reductant, Cu/MWCNT-F-EG and Cu/MWNCT-EG (Fig. 2e and f), give more complex XRD patterns. Neither of the two samples displays the characteristic peaks of Cu or CuO. Instead, they present low intensity peaks corresponding to $Cu(OH)_2$ (00-035-0505) and to Cu_2O [29], the latter phase giving higher intensity peaks in Cu/MWCNT-EG. The formation of Cu(II) hydroxide is ascribed to the preparation method, in which the samples are treated in a water solution at 170 °C.

The surface properties of Cu/Cu_xO nanoparticles were studied by XPS. Fig. 3 shows the Cu 2p XPS spectra of the Cu-containing electrocatalysts. The intensity of the spectrum provides an estimate of the composition in the top 3 nm layer of the material, i.e. on the surface of the material. The XPS signal of Cu 2p contains a main and a satellite peak for Cu $2p_{3/2}$ and $2p_{1/2}$ photoelectrons (see Fig. 3B). The satellite peaks of the Cu $2p_{3/2}$ and $2p_{1/2}$ at 942.4 eV and 962.6 eV, respectively, are an indication of the presence of Cu(II) species [36]. On the other hand, the Cu $2p_{3/2}$ core level provides information about the oxidation state of the Cu atoms: signals at 932.4 ± 0.2 eV, 933.7 ± 0.2 eV, and 934.6 eV are assigned to Cu/Cu_2O, CuO and $Cu(OH)_2$, respectively [37]. Cu and Cu_2O cannot be distinguished in the Cu $2p_{3/2}$ range, because their binding energies are very close to each other [37]. The deconvolution results of Cu $2p_{3/2}$ XPS for the Cu/Cu_xO electrocatalysts are summarized in Table 2. For Cu/MWCNT-F-EG (Fig. 3A.b), and Cu/MWCNT-EG (Fig. 3B.b), the main surface species is $Cu(OH)_2$. In line with the XRD analysis, a small fraction of Cu/Cu_2O is also present in both samples, and the latter has a relatively larger amount of this species (Table 2, compare entry 1 and entry 3). The Cu/Cu_2O phase could be further oxidized to an amorphous layer of CuO in sample Cu/MWCNT-EG. An asymmetric Cu $2p_{3/2}$ peak was observed for Cu/MWCNT-F-H_2 (Fig. 3Aa). Deconvolution of this peak indicates the presence of CuO, $Cu(OH)_2$, and of Cu_2O and/or metallic Cu, species (Table 2, entry 2). The same species were also identified from the XPS spectrum of

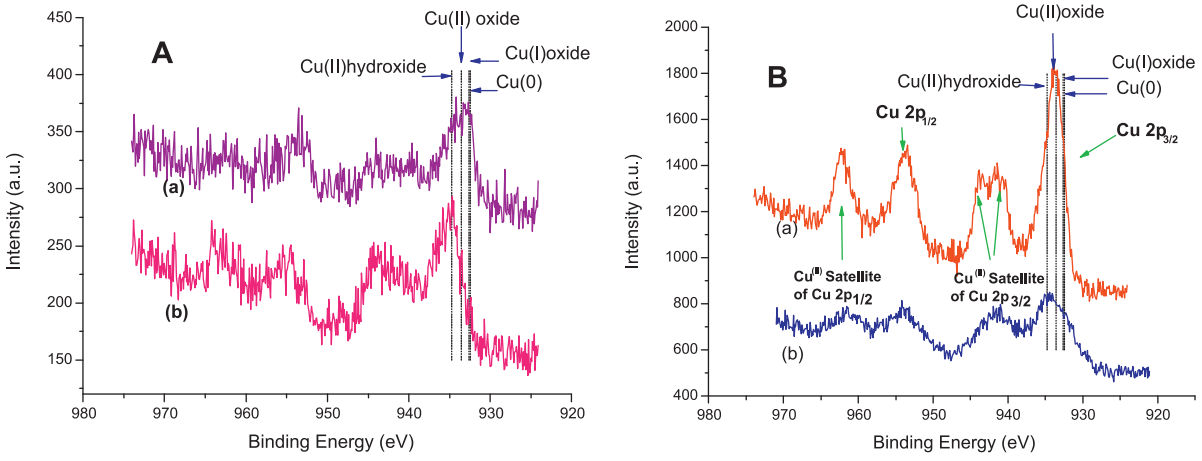

Fig. 3. Cu 2p core level XPS spectra for supported Cu electrocatalyst on MWCNT-F (A): (a) Cu/MWCNT-F-H_2; (b) Cu/MWCNT-F-EG and on MWCNT (B): (a) Cu/MWCNT-H_2; (b) Cu/MWCNT-EG.

Table 2
Binding energies (B.E.) and relative intensities of various species as obtained from the Cu $2p_{3/2}$ XPS of Cu electrocatalysts.

No.	Electrocatalysts	$Cu(OH)_2$		CuO		Cu/Cu_2O	
		B.E. (eV)	area (%)	B.E. (eV)	Area (%)	B.E. (eV)	Area (%)
1	Cu/MWCNT-F-EG	934.7	97.7	–	0	932.4	2.3
2	Cu/MWCNT-F-H_2	934.7	32.9	933.7	38.0	932.6	29.0
3	Cu/MWCNT-EG	934.7	76.7	933.8	6.6	932.2	16.7
4	Cu/MWCNT-H_2	934.7	24.2	933.8	62.0	932.4	13.8

Cu/MWCNT-H_2 (Fig. 3Ba), though in this material the CuO fraction is larger and the Cu/Cu_2O fraction is smaller (Table 2, entry 4). These Cu species were also observed in the XRD patterns of the two materials (vide supra), with the exception of $Cu(OH)_2$. This suggests the presence of an amorphous Cu(II) hydroxide layer located on the surface of the Cu/Cu_xO nanoparticles, which is probably generated upon exposure of the particles to moisture from the atmosphere. The relative content of Cu/Cu_2O in Cu/MWCNT-F–H_2 is higher than in the other Cu-based electrocatalysts (Table 2). This higher relative content of species with Cu in low oxidation state in Cu/MWCNT-F-H_2, can be related to the growth of the Cu/Cu_xO nanoparticles inside the nanotubes (as evidenced by TEM), where they can be protected from oxidation and hydration.

In summary, the physicochemical features of the supported nanoparticles are determined by the different methods employed in their preparation. The method using ethylene glycol as reductant is highly efficient to prepare uniform small-sized Pt nanoparticles with high dispersion, but is not suitable for preparing the supported Cu/Cu_xO nanoparticles. Ethylene glycol is a mild reductant, and its use in an aqueous environment at high temperature is not efficient in generating metallic Cu particles: under these conditions large particles consisting of copper oxide and, mainly, copper hydroxide were obtained. Supported Cu/Cu_xO nanoparticles were successfully obtained with the desired small size and good dispersion with the method employing H_2 as reductant. These Cu/Cu_xO nanoparticles contain both CuO and metallic Cu crystalline phases, as evidenced by XRD, and a surface layer of $Cu(OH)_2$, as shown by XPS, which probably forms on the surface of the nanoparticles in contact with air moisture. Untreated and functionalized MWCNTs were used as support material for Cu/Cu_xO nanoparticles. When the short, open MWCNT-Fs are used as support in the method employing H_2 as reductant, Cu/Cu_xO nanoparticles tend to grow inside the tubes. On the basis of this characterization study, it can be concluded that Pt/MWCNT-F-EG and Cu/MWCNT-H_2 have the most suitable particle size and dispersion for (electro)catalytic applications.

3.2. Electrochemical tests

3.2.1. Electrochemical performance of Cu/Cu_xO and Pt nanoparticles supported on MWCNTs

The activity of the supported nanoparticle electrocatalysts was studied by linear sweep voltammetry (LSV), which is a suitable technique for the investigation of complex multiple-step reactions as the reduction of nitrobenzene [19]. Testing of the electrocatalysts by means of LSV was carried out by varying the potential of the working electrode from −0.3 V to −2.5 V vs. Fc/Fc^+. In Fig. 4, polarization curves for a selected electrocatalyst (Cu/MWCNT-H_2) are shown as an example. Voltammograms of the reduction of nitrobenzene in neutral medium showed an increase of diffusion-limited current density when the rotation rate was increased (500 rpm, 1000 rpm and 1500 rpm). The overall number of electrons transferred per nitrobenzene molecule was studied by the comparison of the slopes of Koutécky–Levich (*K–L*) plots. Fig. 5 shows the *K–L* plots at −1.3 V vs. Fc/Fc^+ for each electrocatalyst, where a smaller slope implies a higher numbers of electrons transferred. The slopes of the *K–L* lines of both Cu/MWCNT-H_2

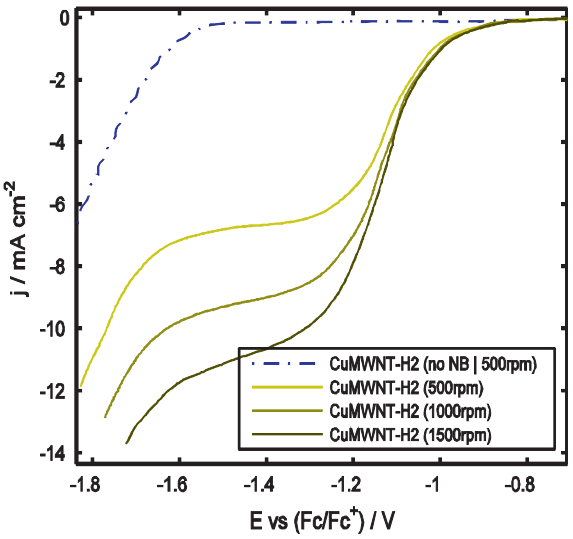

Fig. 4. Linear sweep voltammetry of Cu/MWCNT-H_2 for the reduction of nitrobenzene (5 mM) in 0.2 M $LiClO_4$ ethanolic solution with various rotation speeds. Scan rate was 5 mV s^{-1}. The blank (dotted curve) was measured in the 0.2 M $LiClO_4$ ethanolic solution without nitrobenzene.

and Cu/MWCNT-EG correspond to a 4-electron reduction process, which is identified as the reduction of nitrobenzene to PHA [19]. For the other electrocatalysts, the reduction involved less than 4 electrons. The polarization curve of the electrocatalysts supported on MWCNT-F was not reproducible when repeating the measurement at the same rotation rate. This suggests that reduction of the functional groups on the surface of the nanotubes may occur,

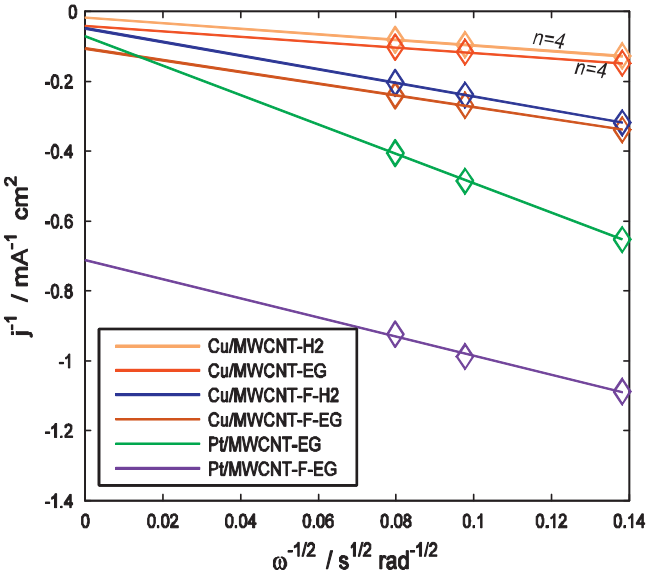

Fig. 5. *K–L* plots of the studied electrocatalysts at −1.3 V vs. Fc/Fc^+ for the determination of the number of electrons transferred during the reduction of nitrobenzene in 0.2 M $LiClO_4$ ethanolic solution.

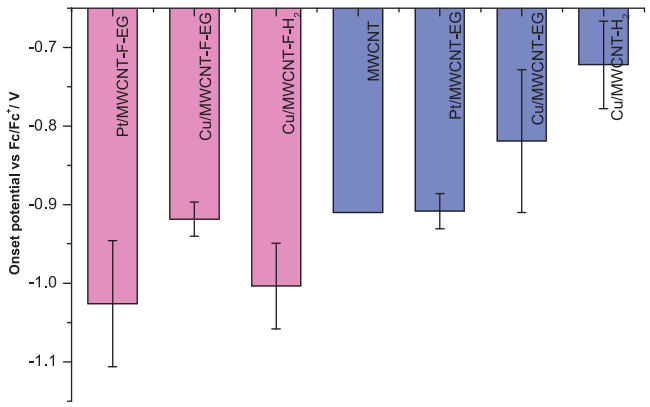

Fig. 6. Onset potential of the studied electrocatalysts supported on MWCNT-F (purple) and on MWCNT (blue) in the nitrobenzene reduction. The values were obtained from the linear sweep voltammograms measured in 0.2 M $LiClO_4$ with a rotation speed of the working electrode of 1500 rpm and a scan rate of 5 mV s^{-1}.(For interpretation of the references to color in this figure legend, the reader is referred to the web version of this article.)

pointing to instability of these electrocatalysts. The slope of the *K–L* line for Pt/MWCNT-EG electrocatalyst is not constant at different potentials, which could mean that the electron transfer on this catalyst is quasi-reversible [38]. As the number of electrons exchanged in the reaction is not the same for all catalysts, the kinetic current cannot be used as a measure of the catalyst activity. Therefore, the onset potential, which is the potential at which the reduction starts, was employed as parameter to evaluate the activity of the electrocatalysts [39]. High electrocatalytic activity will lead to a less negative onset potential. The onset potential was calculated as the potential at which the slope of the voltammogram exceeded 0.1 mA cm^{-2} V^{-1}. The ranking of the studied electrocatalysts based on onset potential (Fig. 6), combined with the number of electrons exchanged, clearly identify Cu/MWCNT-H_2 and Cu/MWCNT-EG as the best performing electrocatalysts for the reduction of nitrobenzene. Since the same number of electrons ($n = 4$) was exchanged when using these two electrocatalysts, it was possible to compare these two materials also on the basis of their kinetic current. The trend of activity based on the onset potential is confirmed by the kinetic current measured at −1.3 V vs. Fc/Fc^+, with Cu/MWCNT-H_2 ($j_K = -31$ mA cm^{-2}) performing better than Cu/MWCNT-EG ($j_K = -19$ mA cm^{-2}). When considering these last data, it should be taken into account that these values of kinetic current were not corrected through the electrochemically active surface area (EASA) and thus include contributions of both intrinsic activity and surface area [40].

The tested electrocatalysts display different onset potential as a function of the features of the nanoparticles and of the support (Fig. 6). The Pt/MWCNT-F-EG electrocatalyst presents a very uniform and small size of the nanoparticles with good dispersion, but its activity based on the onset potential value is lower compared to the electrocatalysts containing Cu, regardless of the method used to prepare them. The supported Pt nanoparticles in Pt/MWCNT-EG, having a very small size with less dispersion and broader size distribution, show less negative onset potential than Pt/MWCNT-F-EG, but still inferior compared to the best Cu/Cu_xO samples. Hence, it can be concluded that the nature of Pt is less suitable than Cu/Cu_xO for catalyzing the electrochemical reduction of nitrobenzene. The actual nature of the copper active sites cannot be determined at this stage. The Cu(II) species (CuO and $Cu(OH)_2$), which are present in all the Cu-containing electrocatalysts are likely to get reduced during the first voltammetric measurement performed in the absence of nitrobenzene, in which reduction of the electrocatalyst was observed (Fig. S.4 in Supporting information). Therefore, metallic copper is expected to be the active species. The better performance of Cu compared to Pt can be ascribed to the more electropositive nature of the former metal. It has been proposed that copper displays a metastable surface redox transition that plays a role in its electrocatalytic activity in the reduction of nitrobenzene and nitrate ions [23].

Although most of the Cu/Cu_xO electrocatalysts perform better than the Pt electrocatalysts, their activity differs as a function of their physical features (Fig. 6). The key factor in determining the order of activity among these electrocatalysts is expected to be the size and distribution of the Cu/Cu_xO nanoparticles: small and well dispersed nanoparticles lead to more exposed sites and larger active areas and thus to better catalytic performances. Indeed, Cu/MWCNT-H_2 was identified as the best Cu electrocatalyst both in terms of its less negative onset potential and of number of electrons exchanged in the reaction (Figs. 5 and 6). This material displays small and highly dispersed Cu/Cu_xO nanoparticles, while the Cu/Cu_xO electrocatalysts prepared with EG contain large aggregates of Cu/Cu_xO particles, resulting in a lower activity. On the other hand, Cu/MWCNT-F-H_2 shows a very poor electrocatalytic performance of (Fig. 6), although it has the similar size and dispersion of Cu/Cu_xO nanoparticles as Cu/MWCNT-H_2. However, most of these particles are located inside the nanotubes, leading to decreased or no accessibility to some particles that are blocked by the presence of other particles in the same tube (see Fig. 1d). Accordingly, the polarization curve of Cu/MWCNT-F-H_2 is very similar to that of MWCNT-F (see Fig. S.3).

The most promising electrocatalyst identified in this work, Cu/MWCNT-H_2, contains both CuO and metallic Cu crystalline phases, with Cu(II) hydroxides species on the surface. In contrast, no or negligible amounts of Cu(0) were identified by XRD and XPS in the less active electrocatalyst (Cu/MWCNT-F-EG). Therefore, metallic Cu may be required to improve the electrical conductivity of the electrocatalyst. Future research work will help to shed more light on the importance of the different Cu phases.

The support material also plays an important role in determining the activity of the electrocatalyst. Compared to MWCNT-F, catalysts supported on the untreated MWCNTs present more negative onset potential (Fig. 6). Moreover, the voltammetric analysis of the electrocatalysts supported on MWCNT-F showed low reproducibility regardless of the metal or the synthetic method. As discussed before, the functional groups on the surface of MWCNT-F might get reduced during the electrochemical reaction or interact with reagents and products, causing the deterioration of the support and the blockage of the active sites, resulting in lower activity and stability than with the untreated MWCNTs. The employed MWCNTs contain a minor amount of residual metal (mainly Co), which is removed during the acid treatment used to prepare MWCNT-F (Table S.1). However, these species do not contribute relevantly to the electrocatalytic activity, as demonstrated by the much more negative onset potential of the MWCNT alone compared to the Cu–Cu_xO electrocatalysts supported on MWCNT (Fig. 6 and Fig. S. 3).

3.2.2. *Stability of Cu/MWCNT-H_2*

The stability of the most promising electrocatalyst, Cu/MWCNT-H_2, was tested with cyclic voltammetry (Fig. 7). No major difference was observed between the voltammogram in the first cycle and that after 1000 cycles, indicating a good stability of the electrocatalyst under the employed conditions. The difference in the cathodic current for the 1st and 1000th cycle is due to the increase in the concentration of reactant, since some of the ethanol evaporated. It can be seen that the activity of the electrocatalyst does not deteriorate over time in this medium (0.2 M $LiClO_4$).

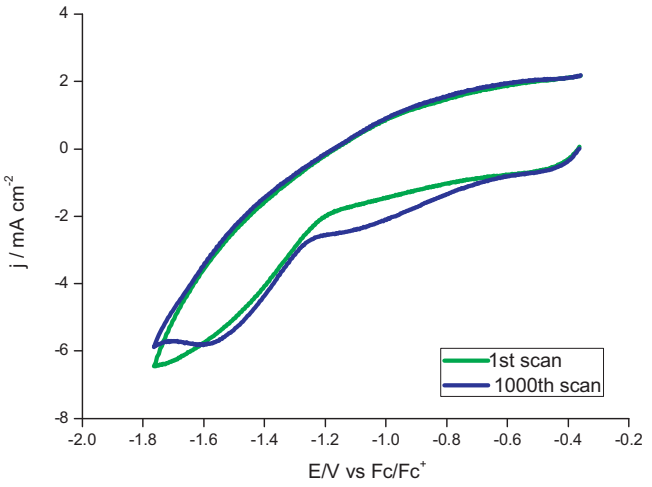

Fig. 7. Stability test of Cu/MWCNT-H_2. The potential was cycled between −0.3 V and −1.7 V vs. Fc/Fc^+. Scan rate was 100 mV s^{-1}. The first (green curve) and last (blue curve) scan are shown. After 999 cycles, the measurement was stopped, the solution was stirred and then the last scan was measured. This procedure allows increasing the comparability of the starting and final reaction conditions. The voltammogram does not show a closed loop because of stopping and restarting the measurement. (For interpretation of the references to color in this figure legend, the reader is referred to the web version of this article.)

3.2.3. Chronoamperometric test for Cu/MWCNT-H_2

The best electrocatalyst identified in this work, Cu/MWCNT-H_2, was evaluated by means of a chronoamperometric test of the reduction of nitrobenzene (15 mM), both in neutral and acidic medium. A more detailed electrochemical study of the reduction of nitrobenzene on a selection of these electrocatalysts is reported elsewhere [19]. For the reaction in neutral medium (0.2 M $LiClO_4$), a potential of −1.15 V (vs. Fc/Fc^+) was employed for 46 h, while −0.62 V (vs. Fc/Fc^+) was used for the reaction in acidic medium (0.3 M $HClO_4$) for 52 h. Potentials were chosen such that a current density for $-2\ mA\ cm^{-2}$ was obtained for both cases. The potential is different because the electrolyte resistance of the two solutions is different. HPLC was used to determine the concentration of chemicals after the reaction. The reaction in neutral medium is slower than in acidic conditions. In neutral medium, the conversion of nitrobenzene is low, only 12.5%, due to the low concentration of protons, which are involved in the reduction process (Scheme 1). The two main products are AOB and aniline, with yields of 9.8% and 2.3%, respectively. Under the acidic conditions used in this study, AOB is the major product of the reduction of nitrobenzene with a yield of 36% and selectivity of 82%. This result and the low yield of aniline indicate that the reduction of nitrobenzene does not proceed further than to PHA with the Cu/MWCNT-H_2 electrocatalyst under these reaction conditions. This mechanism is in agreement with the 4-electron transfer process that was estimated on the basis of the conversion of nitrobenzene (44%) and of the total charge that passed through the system during the reaction [19]. The two major products, AOB and *p*-ethoxyaniline (10% selectivity) can be generated by non-electrochemical reaction of the highly unstable PHA (Scheme 1) [9].

4. Conclusions

Electrocatalysts based on supported Cu/Cu_xO or Pt nanoparticles were synthesized, fully characterized and tested in the reduction of nitrobenzene. Small (3 nm), uniform and well-dispersed Pt nanoparticles supported on functionalized MWCNTs were successfully prepared using ethylene glycol as reductant. However, neither the reductant nor the support proved suitable for preparing a Cu analog. An alternative method, employing hydrogen gas as reductant was efficient in the synthesis of highly dispersed Cu/Cu_xO nanoparticles with an average size of 8 nm supported on untreated MWCNTs. The activities of the synthesized electrocatalysts were evaluated for the electrochemical reduction of nitrobenzene on the basis of their onset potential measured in neutral ethanolic conditions. Remarkably, the inexpensive supported Cu/Cu_xO nanoparticles showed a much better activity than the supported Pt nanoparticles. The Cu/MWCNT-H_2 electrocatalyst has good electrochemical stability, as determined after 1000 cycles in a cyclic voltammetry test. A nitrobenzene conversion of 44% was achieved with this electrocatalyst after 52 h of reaction at room temperature in ethanol with $HClO_4$ as electrolyte at −0.62 V vs. Fc/Fc^+. AOB was identified as the major product of the reaction, with a selectivity of 82%. The formation of this compound can be ascribed to the further reaction of PHA, obtained by the reduction of nitrobenzene.

In future perspective, the Cu/MWCNT-H_2 electrocatalyst is a promising candidate for the development of a fuel cell that is able to cogenerate electricity and useful products from the reduction of nitrobenzene.

Acknowledgments

The authors acknowledge sponsoring from the Flemish Agency for Innovation by Science and Technology (I.W.T.) in the frame of an S.B.O. project (OCPEC), and are grateful for support by VITO Research Center. We thank Dr. Heidi Van Parys, Kitty Baert and Oscar Steenhaut for their help with SEM-EDX and XPS measurements. We acknowledge Dr. Chalida Klaysom for TEM operation, the MTM Department of the KU Leuven for TEM Technical Support and the Flemish Hercules Stichting for its support in HER/08/25. We thank Prof. Christine Kirschhock and Dr. Elena Gobechiya for assistance in the XRD analysis. We acknowledge support by the IAP-PAI Research Program.

Appendix A. Supplementary data

Supplementary data associated with this article can be found, in the online version, at http://dx.doi.org/10.1016/j.apcatb.2013.09.006.

References

[1] X.-Z. Yuan, H. Wang, in: J. Zhang (Ed.), PEM Fuel Cell Electrocatalysts and Catalyst Layers Fundamentals and Applications, Springer-Verlag, London, 2008, Chapter 1.
[2] X.Z. Yuan, Z.F. Ma, Q.Z. Jiang, W.S. Wu, Electrochemistry Communications 3 (2001) 599–602.
[3] T. Niknam, M. Bornapour, A. Gheisari, B. Bahmani-Firouzi, International Journal of Hydrogen Energy 38 (2013) 1111–1127.
[4] X.C. Meng, H.Y. Cheng, Y. Akiyama, Y.F. Hao, W.B. Qiao, Y.C. Yu, F.Y. Zhao, S. Fujita, M. Arai, Journal of Catalysis 264 (2009) 1–10.
[5] E. Merino, Chemical Society Reviews 40 (2011) 3835–3853.
[6] J.W. Larsen, M. Freund, K.Y. Kim, M. Sidovar, J.L. Stuart, Carbon 38 (2000) 655–661.
[7] A. Furst, R.C. Berlo, S. Hooton, Chemical Reviews 65 (1965) 51–68.
[8] J. Jiang, R. Zhai, X. Bao, Journal of Alloys and Compounds 354 (2003) 248–258.
[9] K.P. Naicker, K. Pitchumani, R.S. Varma, Catalysis Letters 58 (1999) 167.
[10] A.R. Becker, L.A. Sternson, Proceedings of the National Academy of Sciences of the United States of America—Physical Sciences 78 (1981) 2003–2007.
[11] G. Kokkinidis, K. Jüttner, Electrochimica Acta 26 (1981) 971–977.
[12] D. Grošková, M. Štolcová, M. Hronec, Catalysis Letters 69 (2000) 113–116.
[13] A. Cyr, P. Huot, J.F. Marcoux, G. Belot, E. Laviron, J. Lessard, Electrochimica Acta 34 (1989) 439–445.
[14] A. Cyr, P. Huot, G. Belot, J. Lessard, Electrochimica Acta 35 (1990) 147–152.
[15] P.N. Pintauro, J.R. Bontha, Journal of Applied Electrochemistry 21 (1991) 799–804.
[16] O.S.G.P. Soares, J.J.M. Órfão, M.F.R. Pereira, Industrial & Engineering Chemistry Research 49 (2010) 7183–7192.
[17] W.Y. Xu, T.Y. Gao, J.H. Fan, Journal of Hazardous Materials 123 (2005) 232–241.
[18] A. Saha, B. Ranu, Journal of Organic Chemistry 73 (2008) 6867–6870.

[19] B. Wouters, X. Sheng, A. Boschin, T. Breugelmans, E. Ahlberg, I.F.J. Vankelecom, P.P. Pescarmona, A. Hubin, Electrochimica Acta (2013), http://dx.doi.org/10.1016/j.electacta.2013.07.210.
[20] C. Yu, S. Koh, J.E. Leisch, M.F. Toney, P. Strasser, Faraday Discussions 140 (2008) 283–296.
[21] D. Villers, S.H. Sun, A.M. Serventi, J.P. Dodelet, S. Desilets, Journal of Physical Chemistry B, Focus on Physics 110 (2006) 25916–25925.
[22] H. Wang, Q. Pan, J. Zhao, W. Chen, Journal of Alloys and Compounds 476 (2009) 408–413.
[23] L.D. Burke, R. Sharna, Journal of Applied Electrochemistry 37 (2007) 1119–1128.
[24] W.-M. Chiu, Y.-A. Chang, Journal of Applied Polymer Science 107 (2008) 1655–1660.
[25] Z.H. Zhou, S.L. Wang, W.J. Zhou, G.X. Wang, L.H. Jiang, W.Z. Li, S.Q. Song, J.G. Liu, G.Q. Sun, Q. Xin, Chemical Communications (2003) 394–395.
[26] G. Yu, W. Chen, J. Zhao, Q. Nie, Journal of Applied Electrochemistry 36 (2006) 1021–1025.
[27] K. Bouzek, K.M. Mangold, K. Jüttner, Journal of Applied Electrochemistry 31 (2001) 501–507.
[28] V. Radmilović, H.A. Gasteiger, P.N. Ross, Journal of Catalysis 154 (1995) 98–106.
[29] International Center for Diffraction Data, Reference Code (PDF2008), 2008, 00-004-0836, 01-080-1916, 01-071-3645, 00-035-0505.
[30] Y.-C. Chiang, W.-H. Lin, Y.-C. Chang, Applied Surface Science 257 (2011) 2401–2410.
[31] X. Li, Y. Liu, L. Fu, L. Cao, D. Wei, Y. Wang, Advanced Functional Materials 16 (2006) 2431–2437.
[32] Y. Huang, J. Liao, C. Liu, T. Lu, W. Xing, Nanotechnology 20 (2009).
[33] X. Wang, M. Waje, Y.S. Yan, Electrochemical and Solid State Letters 8 (2005) A42–A44.
[34] R. Mohan, A.M. Shanmugharaj, R.S. Hun, Journal of Biomedical Materials Research Part B—Applied Biomaterials 96B (2011) 119–126.
[35] Z. Ai, H. Xiao, T. Mei, J. Liu, L. Zhang, K. Deng, J. Qiu, Journal of Physical Chemistry C 112 (2008) 11929–11935.
[36] O. Akhavan, R. Azimirad, S. Safa, E. Hasani, Journal of Materials Chemistry 21 (2011) 9634–9640.
[37] O. Ghodbane, L. Roue, D. Belanger, Chemistry of Materials 20 (2008) 3495–3504.
[38] D. Jahn, W. Vielstich, Journal of the Electrochemical Society 109 (1962) 849–852.
[39] J.L. Zhang, J.J. Zhang, in: J. Zhang (Ed.), PEM Fuel Cell Electrocatalysts and Catalyst Layers Fundamentals and Applications, Springer-Verlag, London, 2008, pp. 978–984, Chapter 21.
[40] R.F. Savinell, R.L. Zeller, J.A. Adams, Journal of the Electrochemical Society 137 (1990) 489–494.